Influence of the relative refractive index on the depolarization of multiply scattered waves

A. D. Kim* and M. Moscoso†
Department of Mathematics, Stanford University, Stanford, California 94305-2125
(Received 8 December 2000; revised manuscript received 16 March 2001; published 24 July 2001)

Using the theory of radiative transfer, we investigate the interaction between polarized waves and a multiple scattering medium as functions of the relative index of refraction. To study this problem, we consider circularly and linearly polarized continuous waves incident upon a medium containing spherical scatterers. With an accurate spectral method, we compute the transmitted Stokes parameters through media containing different sized scatterers and different indices of refraction. Our numerical results show that the circular depolarization length exhibits a strong dependence on the relative index of refraction, while the linear depolarization length does not.

DOI: 10.1103/PhysRevE.64.026612 PACS number(s): 42.25.Dd, 42.25.Ja, 42.68.Ay

I. INTRODUCTION

Recently, a large number of studies have been reported addressing polarization properties of waves scattered by a turbid medium. The interaction of waves with an inhomogeneous medium not only randomizes the direction of the waves but also their polarization state. It has been shown that the polarization information of an incident polarized source is preserved over long distances, and that the characteristic length over which it depolarizes depends on the size of the inhomogeneities compared with the wavelength [1,2]. Similar results have been found using time-resolved measurements [3]. For spatial inhomogeneities that are small compared with the wavelength, linear polarization is preserved over slightly larger distances than circular polarization [2]. On the other hand, circular polarization is maintained over larger distances for spatially large inhomogeneities [2,4].

In addition to size dependence, we show that polarization properties of waves interacting with an inhomogeneous medium also depend on the relative index of refraction (the ratio between the indices of refraction of the inhomogeneities and the background). In particular, we consider a medium composed of optically inactive spherical scatterers, and we numerically study the depolarization of light transmitted through the medium for different sphere sizes and refractive indices. Our computations show that depolarization lengths can strongly depend on the relative refractive index.

Included in this study is the case where the relative refractive index is close to 1. This is an important case for many applications such as ocean [5–7], atmospheric [8–11] and biological optics [12–14]. The random fluctuations of the refractive index in the sea and the atmosphere are due to temperature variations. Salinity fluctuations in the sea and humidity fluctuations in the atmosphere also lead to small relative variations in the refractive index. These effects yield refractive index variations on the order of 1% or less. The variations in soft tissues due to structures within cells are of the order of 5% [15].

*Electronic address: adkim@math.stanford.edu
†Electronic address: mmoscoso@math.stanford.edu

II. RADIATIVE TRANSFER THEORY

The theory of radiative transfer models waves propagating in a scattering and absorbing medium. This theory is appropriate for problems in which propagation distances are much larger than the wavelength. For polarized waves, radiative transfer uses the four Stokes parameters I, Q, U, and V. The total intensity is represented by I, the linear polarization state by Q and U, and the circular polarization state by V. The vector radiative transfer equation

$$\frac{1}{v}\frac{\partial \mathbf{I}(\mathbf{x},\hat{\Omega},t)}{\partial t}+\hat{\Omega}\cdot\nabla_x\mathbf{I}(\mathbf{x},\hat{\Omega},t)+\Sigma_a\mathbf{I}(\mathbf{x},\hat{\Omega},t)$$
$$=-\Sigma_s\left[\mathbf{I}(\mathbf{x},\hat{\Omega},t)-\int F(\hat{\Omega},\hat{\Omega}')\mathbf{I}(\mathbf{x},\hat{\Omega}',t)d\hat{\Omega}'\right], \quad (1)$$

governs the 4×1 Stokes vector $\mathbf{I}=(I,Q,U,V)$, which depends on position $\mathbf{x}$, direction $\hat{\Omega}$, and time t. Here v is the constant wave speed, Σ_s is the scattering cross section, and Σ_a is the absorption cross section. The integral operation in Eq. (1) that involves the 4×4 scattering matrix $F(\hat{\Omega},\hat{\Omega}')$ takes place over the unit sphere. This scattering matrix describes the directional distribution of waves that scatter in direction $\hat{\Omega}$ due to waves of unit energy density incident in direction $\hat{\Omega}'$. In addition, it describes polarization changes that waves undergo after scattering. If the scattering matrix F uses the scattering plane as its plane of reference, it depends only on the cosine of the scattering angle Θ.

If the medium contains spherical scatterers, the scattering matrix can be computed exactly using Mie theory. In this case, all the elements of F are functions of the nondimensional size parameter ka (k is the wave number in the background medium, and a the radius of the scatterers) and of the relative refractive index m.

Two limits are particularly interesting here: $ka\ll1$ and $|m-1|\ll1$. When $ka\ll1$ the Rayleigh scattering limit is valid regardless of the value of m [16]. We denote the scattering matrix in this limit by R. On the other hand, for $|m-1|\ll1$, the scattering matrix is simply the product of R and a scalar function that does not depend on polarization. This is the Rayleigh-Gans limit [16]. The scalar function

governs the amount of energy that scatters in the forward direction and is a function of *ka*. The Rayleigh-Gans range is not limited to homogeneous discrete spherical particles. Scatterers with simple forms such as ellipsoids or spheroids as well as inhomogeneous density distributions can also be treated. Furthermore, if the scatterers are not compactly supported in space (continuous random media), and the relative refractive index fluctuations are small, the scattering matrix F takes a form similar to that of the Rayleigh-Gans limit. In this case, the scalar function multiplying R is the power spectral density function of the fractional permittivity fluctuations which incorporates the statistical properties of the medium [17]. The physical basis of the Rayleigh-Gans limit is that the wave fields scattered from different small volumes within the medium are always independent.

In many applications the vector radiative transport equation (1) is approximated by its scalar counterpart. In this approximation polarization is neglected, so $Q=U=V=0$ in Eq. (1), and the 4×4 matrix is replaced by a scalar function $p(\hat{\Omega},\hat{\Omega}')$ called the phase function. The phase function is often characterized by the anisotropy factor g. For example, the Henyey-Greenstein phase function

$$p(\hat{\Omega},\hat{\Omega}')=\frac{1-g^2}{2(1-g^2+2g\cos\Theta)^{2/3}} \tag{2}$$

is often used to describe scattering from clouds and tissues [18]. Here $\cos\Theta=\hat{\Omega}\cdot\hat{\Omega}'$. This function varies smoothly from isotropic scattering ($g=0$) to narrow forward peak scattering ($g\sim1$) or backward peak scattering ($g\sim-1$). Within this scalar approximation only three parameters are necessary to match the observed intensity of a particular experiment: the scattering coefficient Σ_s, the absorption coefficient Σ_a, and the anisotropy factor g characterizing the phase function.

However, we will show that the relative refractive index also affects depolarization. Different media with similar Σ_s,Σ_a, and g values can exhibit distinctly different polarization characteristics if the relative refractive index is different. Consequently, the entire structure of the scattering matrix and its dependence on the scatterer size and refractive index need to be considered to understand the depolarization of waves in a scattering medium.

III. NUMERICAL RESULTS

We begin this numerical investigation by examining the anisotropy factor of a single sphere. In Fig. 1(a) we plot the anisotropy factor

$$g=2\pi\int_{-1}^{1}\cos\Theta F_{11}(\cos\Theta)d(\cos\Theta), \tag{3}$$

computed from Mie theory for $m=1.01$ (solid line), $m=1.20$ (dashed line), and $m=1.40$ (dot-dashed line) as functions of the size parameter *ka*. Here F_{11} is the (1, 1) element of the scattering matrix F. We observe that the behavior of g is similar for $1.0<m<1.2$. In contrast, the anisotropy factor is not a monotonic function of *ka* for $m=1.40$. The complicated behavior of g reflects the characteristic oscillations of Mie resonances. Also interesting is the fact that for large relative refractive indices and large size parameters, the anisotropy factor is diminished. This behavior is due to the increase of backscattering as the relative refractive index increases.

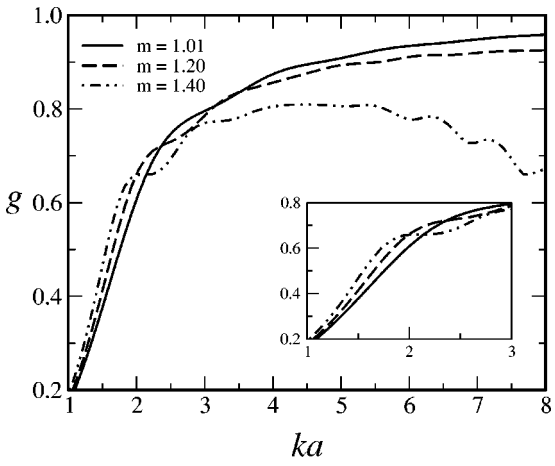

FIG. 1. Anisotropy factor g as a function of the nondimensional size parameter *ka* for a medium composed of spherical scatterers with relative refractive indexes $m=1.01$ (solid line), $m=1.20$ (dashed line), and $m=1.40$ (dot-dashed line). The inset enlarges the region $1\leqslant ka\leqslant3$.

In our numerical simulations, we consider either a 100% circular or 100% linear polarized continuous plane wave normally incident upon an index-matched plane-parallel medium of optical thickness $\tau=d/l$, where d is the physical thickness and $l=(\Sigma_{sc}+\Sigma_a)^{-1}=\Sigma_t^{-1}$ is the total mean free path. In this case Eq. (1) reduces to

$$\cos\theta\frac{\partial}{\partial z}\mathbf{I}(z,\theta,\phi)+\Sigma_a\mathbf{I}(z,\theta,\phi)$$
$$=-\Sigma_s\left[\mathbf{I}(z,\theta.\phi)-\int_0^{2\pi}\int_0^{\pi}F(\theta,\phi,\theta',\phi')\right.$$
$$\left.\times\mathbf{I}(z,\theta',\phi')\sin\theta'\,d\theta'\,d\phi'\right]. \tag{4}$$

Here θ is the polar angle defined with respect to the z axis, and ϕ is the azimuthal angle. This plane-parallel medium contains a random distribution of dielectric spheres, each with a constant radius a and a relative refractive index m. Therefore, the scattering matrix is computed exactly using Mie theory [19]. We solve Eq. (4) using a Chebyshev spectral method in which the spatial variable of the Stokes vector $\mathbf{I}$ is approximated by an expansion of Chebyshev polynomials [20]. The resultant system of integral equations for the angularly dependent expansion coefficients is treated by Gaussian quadrature methods, yielding a sparse linear system of equations. This method provides very accurate solutions to Eq. (4). Recently, we also showed that Chebyshev spectral methods are suitable to generalizations of Eq. (4) including time dependent and higher dimensional problems [21]. While Eq. (4) offers a significant simplification to the general problem [Eq. (1)], we found that polarization prop-

erties from these results agree well with Monte Carlo simulations of more complicated problems involving finite width beams. Therefore, we use Eq. (4) as a simple model from which we are able to ascertain fundamental polarization phenomena.

The transmitted copolarized I_{copol} and cross-polarized $I_{x\text{-pol}}$ intensities are computed in each case with respect to a receiver with a 16° semiaperature directed normal to the boundary plane at $z=d$. The copolarized intensity is the received intensity, having the same direction of polarization as the incident wave. For linear (circular) polarization, the transmitted cross-polarized component is perpendicular (opposite) to the incident polarization direction. If the medium is completely homogeneous, then there is no scattering, and the transmitted cross-polarized component is zero. However, if the medium is not homogeneous, waves interact with the inhomogeneities, resulting in an increment of cross-polarized component and a decrement of the copolarized component. In Fig. 2(a), we plot the copolarized (solid line) and cross-polarized (dashed line) components as functions of the optical thickness τ for circularly continuous incident plane waves. Figure 2(b) shows the same computation but for linearly incident plane waves. In this case, we have taken into account the fact that we measure the linear polarized intensities with a receiver directed normal the boundary plane. The transmitted intensities I_{copol} and $I_{x\text{-pol}}$, polarized parallel and perpendicular to the incident polarized wave, require a change of basis of the solution vector $\mathbf{I}=(I,Q,U,V)$ to the reference frame of the receiver [19]:

$$I_{\text{copol}}=\tfrac{1}{2}[\cos^2\theta\cos^2\phi+\sin^2\phi]I+\tfrac{1}{2}[\cos^2\theta\cos^2\phi-\sin^2\phi]Q-\tfrac{1}{2}[\cos\theta\sin 2\phi]U, \tag{5a}$$

$$I_{x\text{-pol}}=\tfrac{1}{2}[\cos^2\theta\sin^2\phi+\cos^2\phi]I+\tfrac{1}{2}[\cos^2\theta\sin^2\phi-\cos^2\phi]Q+\tfrac{1}{2}[\cos\theta\sin 2\phi]U. \tag{5b}$$

Note that Eq. (5) may yield a nonzero cross-polarized component due to transmitted intensities in nonforward directions, $\cos\theta\neq 1$.

For an optical thickness $\tau\gg 1$, the normalized polarization difference exponentially decays as

$$\frac{I_{\text{copol}}-I_{x\text{-pol}}}{I_{\text{copol}}+I_{x\text{-pol}}}\sim\exp[-\tau/\xi_i], \tag{6}$$

where the subindex $i=L,C$ denotes linear and circular incident light, respectively. The depolarization lengths defined here are scaled with respect to the total mean free path. The insets in Figs. 2(a) and 2(b), for circularly and linearly polarized waves, respectively, show the exponential decay of their normalized polarization differences. By computing a least-squares fit of the normalized polarization difference data, we obtain the depolarization lengths ξ_C and ξ_L shown below. We note that the normalized polarization difference is used to obtain better optical images of biological media [12,22–24].

In Fig. 3(a) we plot the circular depolarization length ξ_C as a function of the nondimensional size parameter ka for

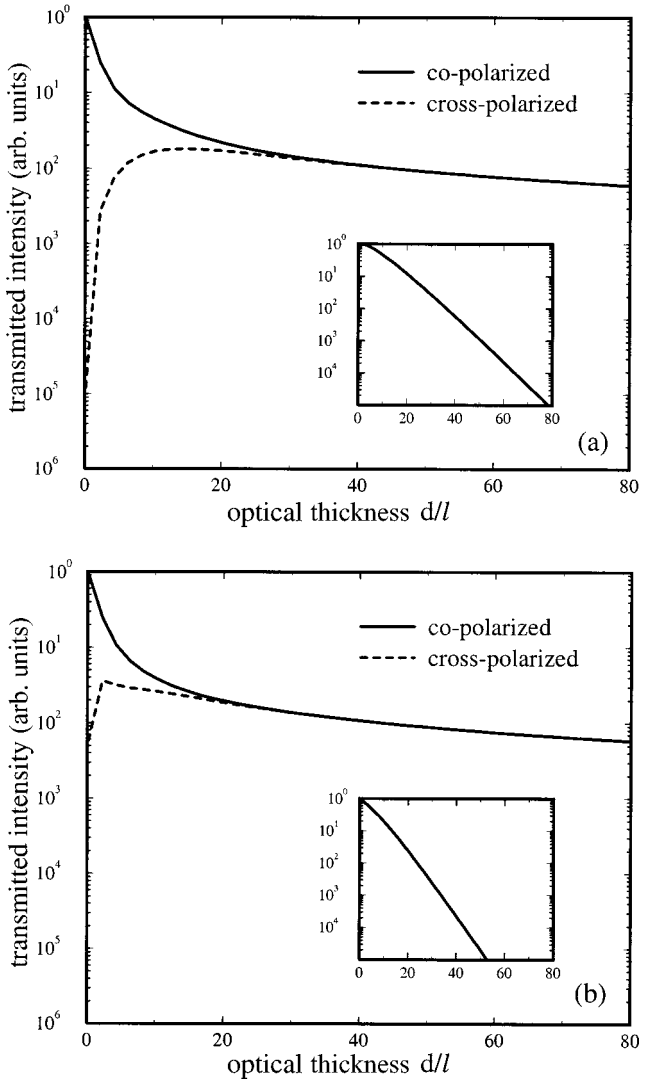

FIG. 2. Transmitted intensities for circularly (a) and linearly (b) polarized incident waves. Here $ka=2.98$ and $m=1.20$. The receiver, which has a 16° field of view, is directed normal to the boundary plane. The inset is a plot showing the exponential decay of the corresponding normalized polarization difference defined in Eq. (6).

three relative indices of refraction m. For small ka we observe that the depolarization length is independent of m, which is consistent with the Rayleigh limit. However, for larger size parameters, ξ_C increases as the relative index of refraction increases. In fact, for $ka=2$ the circular depolarization length for $m=1.40$ is more than two times larger than that for $m=1.01$. The increase of g with respect to m at $ka=2$ is not large enough to explain this effect (see the inset in Fig. 1). Furthermore, for $ka=3$ the circular depolarization length for $m=1.40$ is still much larger than that for $m=1.01$, even though g is nearly equal. We also observe that while ξ_C is simply an increasing function of ka for $m=1.01$, the behavior of ξ_C is more complicated for larger m, reflecting resonance effects.

On the other hand, we observe in Fig. 3(b) that the linear depolarization length ξ_L depends on m more smoothly. Its

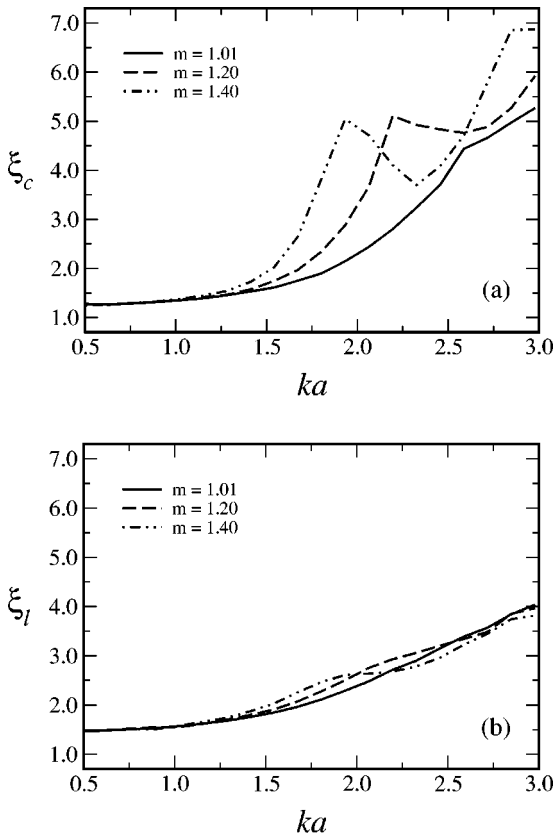

FIG. 3. Circular (a) and linear (b) depolarization lengths ξ_C and ξ_L, respectively, scaled by the scattering mean free path for spherical scatterers with relative refractive indexes $m=1.01$ (solid line), $m=1.20$ (dashed line), and $m=1.40$ (dot-dashed line). The receiver, which has a 16° field of view, is directed normal to the boundary plane.

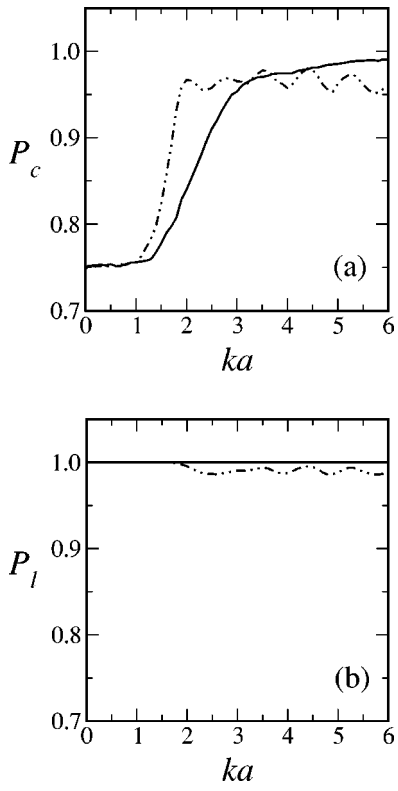

FIG. 4. Fraction of power with circular (a) and linear (b) polarizations scattered from a single sphere due to fully circularly and linearly polarized, incident waves, respectively, as functions of the size parameter for $m=1.01$ (solid line) and $m=1.4$ (dot-dashed line).

behavior can be explained by the anisotropy factor, since ξ_L increases proportionally with g. In contrast with previous results [2], our computations do not show that the ratio ξ_C/ξ_L is an increasing function of ka in general. This ratio increases monotonically with ka only for the case where $|m-1| \ll 1$.

To understand the mechanisms contributing to the depolarization of waves, in Fig. 4 we plot the relative amount of power with circular and linear polarizations scattered by a single sphere due to fully polarized incident plane waves. In Fig. 4(a), we consider a circularly polarized incident wave with Stokes vector $\mathbf{I}=(1,0,0,1)$, impinging on a scatterer with relative indexes of refraction $m=1.01$ (solid line) and $m=1.40$ (dot-dashed line). We compute the relative amount of energy density scattered that is circularly polarized:

$$P_C = \int |V(\Omega')| d\Omega' \Big/ \int I(\Omega') d\Omega'. \tag{7}$$

This quantity ranges from $0 \leqslant P_C \leqslant 1$. It is equal to zero for unpolarized waves, and is equal to 1 for completely circularly polarized waves. In Fig. 4(a), P_C shows a strong dependence on both the size parameter and the relative index of refraction. For $|m-1| \ll 1$ (solid line), P_C grows monotonically to 1. If the relative index of refraction is larger (dot-dashed line), then, after a fast increase, P_C oscillates with a decreasing tendency. In fact, P_C is smaller for a large relative index of refraction than for small ones if the size parameter is large. This phenomenon indicates that circularly polarized waves depolarize faster as m increases for large ka. Our numerical simulations demonstrate this behavior.

Similarly, we consider a linearly polarized incident plane wave with Stokes vector $\mathbf{I}=(1,1,0,0)$ in Fig. 4(b). In this case the Stokes components Q and U are related to each other through rotations, so we consider both together. The relative amount of energy density scattered that is linearly polarized is [25]

$$P_L = \int \sqrt{Q^2(\Omega') + U^2(\Omega')} d\Omega' \Big/ \int I(\Omega') d\Omega'. \tag{8}$$

This quantity also takes values $0 \leqslant P_L \leqslant 1$.

The salient feature of Fig. 4 is that while the P_L is equal or almost equal to 1 regardless of the size parameter or the relative index of refraction, P_C depends on both and is significantly less than 1. As a result, circularly polarized waves will systematically depolarize after each scattering.

Since $P_L \approx 1$, after single scattering, linearly polarized waves are not systematically depolarized like circularly polarized waves. A second mechanism is responsible for linear depolarization. Linear polarization is defined with respect to

a reference plane. For our discussion, let us choose that plane to be the scattering plane spanned by the incident and scattered direction vectors. After several scattering events, the directional distribution of the Stokes vector becomes randomized along with the orientation of these scattering planes. Hence the Stokes vector at any position involves the mixture of several directions, each having different scattering planes, thereby giving rise to depolarization. Consequently, the linear depolarization length is approximately equal to the transport mean free path $l_{\mathrm{tr}}=[\Sigma_t(1-g)]^{-1}$, which is the characteristic length scale for directional randomization. Our numerical results are consistent with this statement. Unlike linear polarization, circular polarization is defined independent of a reference plane, so this second mechanism does not depolarize them.

IV. SUMMARY

In summary, we have studied the influence of the relative refractive index on the depolarization properties of scattering media. By computing solutions to the plane-parallel problem with linearly and circularly polarized incident waves, we determine the corresponding linear and circular depolarization lengths from the exponential decay of the normalized polarization difference. In particular, we find that the circular depolarization length strongly depends on the refractive index. Scattering from a single sphere clearly demonstrates this dependence. While circular depolarization systematically decreases after each scattering event, linear depolarization decreases with the randomization of directions. Consequently, the linear depolarization length is approximately equal to the transport mean free path. This is true independent of the size parameter and the refractive index of the scatterers. In addition, we have observed similar phenomena for various receiver apertures, including a full field of view. These results may be useful for polarization techniques in optical imaging applications.

ACKNOWLEDGMENTS

A.D.K. would like to acknowledge support from the NSF (Grant No. DMS-0071578). M.M. acknowledges support from the AFOSR (Grant No. 49620-98-1-0211) and by the NSF (Grant No. 9709320).

[1] F. C. Mackintosh, J. X. Zhu, D. J. Pine, and D. A. Weitz, Phys. Rev. B **40**, 9342 (1989).
[2] D. Bicout, C. Brosseau, A. S. Martinez, and J. M. Schmitt, Phys. Rev. E **49**, 1767 (1994).
[3] K. M. Yoo and R. R. Alfano, Phys. Lett. A **142**, 531 (1989).
[4] E. E. Gorodnichev, A. I. Kuzovlev, and D. B. Rogozkin, Laser Phys. **9**, 1210 (1999).
[5] G. D. Gilbert and J. C. Pernicka, Appl. Opt. **6**, 741 (1967).
[6] L. E. Mertens and F. S. Replogle, Jr., J. Opt. Soc. Am. A **67**, 1105 (1977).
[7] M. P. Rowe, E. N. Pungh, Jr., J. S. Tyo, and N. Engheta, Opt. Lett. **20**, 608 (1995).
[8] J. S. Ryan and A. I. Carswell, J. Opt. Soc. Am. A **68**, 900 (1978).
[9] C. Werner, J. Streicher, H. Herrmann, and H. G. Dahn, Opt. Eng. **31**, 1731 (1992).
[10] G. W. Kattawar and G. N. Plass, Appl. Opt. **7**, 1519 (1968).
[11] T. Aruga and T. Igarashi, Appl. Opt. **20**, 2698 (1981).
[12] S. G. Demos and R. R. Alfano, Appl. Opt. **36**, 150 (1997).
[13] V. Sankaran, K. Schönonberger, J. T. Walsh, Jr., and D. J. Maitland, Appl. Opt. **38**, 4252 (1999).
[14] M. Moscoso, J. B. Keller, and G. Papanicolaou, J. Opt. Soc. Am. A **18**, 948 (2001).
[15] J. M. Schmitt and G. Kumar, Opt. Lett. **21**, 1310 (1996).
[16] H. C. Van de Hulst, *Light Scattering by Small Particles* (Dover, New York, 1981).
[17] L. Ryzhik, G. Papanicolaou, and J. B. Keller, Wave Motion **24**, 327 (1997).
[18] A. Ishimaru, *Wave Propagation and Scattering in Random Media* (IEEE, New York, 1997).
[19] R. L.-T. Cheung and A. Ishimaru, Appl. Opt. **21**, 3792 (1982).
[20] A. D. Kim and A. Ishimaru, J. Comput. Phys. **152**, 264 (1999).
[21] A. D. Kim and M. Moscoso (unpublished).
[22] J. M. Schmitt, A. H. Gandjbakhche, and R. F. Bonner, Appl. Opt. **31**, 6535 (1992).
[23] S. L. Jacques, J. R. Roman, and K. Lee, Lasers Surg. Med. **26**, 119 (2000).
[24] S. G. Demos, H. B. Radousky, and R. R. Alfano, Opt. Express **7**, 23 (2000).
[25] G. Bal and M. Moscoso, J. Quant. Spectrosc. Radiat. Transfer **70**, 75 (2001).